J. Ocean Univ. China (Oceanic and Coastal Sea Research)
https://doi.org/10.1007/s11802-018-3489-7
ISSN 1672-5182, 2018 17 (1): 186-194
http://www.ouc.edu.cn/xbywb/
E-mail:xbywb@ouc.edu.cn

Crustal Structure Revealed by a Deep Seismic Sounding Profile of Baijing-Gaoming-Jinwan in the Pearl River Delta

ZHANG Xiang[1), 2), 3)], YE Xiuwei[3), *], LV Jinshui[3)], SUN Jinlong[1)], and WANG Xiaona[3)]

1) *CAS Key Laboratory of Ocean Geology*, *South China Sea Institute of Oceanology*, *Chinese Academy of Sciences*, *Guangzhou* 510301, *China*
2) *University of Chinese Academy of Sciences*, *Beijing* 100049, *China*
3) *Guangdong Earthquake Agency*, *China Earthquake Administration*, *Guangzhou* 510070, *China*

(Received March 20, 2017; revised August 28, 2017; accepted October 17, 2017)

Abstract The Pearl River Estuary area, located in the middle part of the southern China coastal seismic belt, has long been considered a potential source of strong earthquakes above magnitude 7.0. To scientifically assess the potential strong earthquake risk in this area, a three-dimensional artificial seismic sounding experiment, consisting of a receiving array and seabed seismograph, was performed to reveal the deep crustal structure in this region. We used artificial ship-borne air-gun excitation shots as sources, and fixed and mobile stations as receivers to record seismic data from May to August 2015. This paper presents results along a line from the western side of the Pearl River Estuary to the western side of the Baijing-Gaoming-Jinwan profile. A two-dimensional velocity structure was constructed using seismic travel-time tomography. The inversion results show that the Moho depth is 27 km in the coastal area and 30 km in the northwest of the Pearl River Estuary area, indicating that the crust thins from land to sea. Two structural discontinuities and multiple low-velocity anomalies appear in the crustal section. Inside both discontinuity zones, a low-velocity layer, with a minimum velocity of 6.05 km s^{-1}, exists at a depth of about 15 km, and another, with a minimum velocity of 6.37 km s^{-1}, exists at a depth of about 21.5 km between the middle and lower crust. These low velocities suggest that the discontinuities may consist of partly molten material. Earthquakes with magnitudes higher than 5.0 occurred in the low-velocity layer along the profile. The deep Kaiping-Enping fault, rooted in the crust, may be one of the most important channels for deep material upwelling and is related to tectonic movement since the Cretaceous in the Pearl River Delta tectonic rift basin.

Key words Pearl River Estuary; seismic sounding profile; crustal structure; Kaiping-Enping fault; earthquake potential

1 Introduction

Pearl River Delta, an important economically developed and densely populated region, plays a decisive role in China's economic and social development status. This special area is located at the center of the active in-board southern China coastal seismic belt. Throughout history there have been many strong earthquakes of magnitude 7.0, such as the NanAo earthquake in 1600, the Qionghai earthquake in 1605, and the NanPeng earthquake in 1918. All caused great damage to economic and social development in the coastal areas of southern China (Xu *et al*., 2006; Zhong and Ren, 2003; Chen and Huang, 1979). The Pearl River Estuary area is located in the middle of the seismic belt, and the historical record shows that no earthquakes greater than magnitude 6.0 have occurred. By comparing the epicentral positions on the seismic belt of magnitude 7.0 or above earthquakes, some investigators found that the Pearl River Estuary area is located in a quiet zone of the seismic belt (Sun *et al*., 2012). Therefore, it has been proposed that this is a potential strong earthquake source area (Wei *et al*., 2000; China Earthquake Parameters Zoning Map, 2015). Many scientists are investigating the geological structure of this area to understand its earthquake potential.

Strong intraplate earthquakes show complex seismogenic mechanisms and source region structures (Talwani, 2016). It is generally believed that the occurrence of strong earthquakes is related to stress concentration along a fracture or petrophysically abrupt interface (Kenner, 2000; Talwani, 2014). According to previous studies, the earthquakes in 1609 and 1918 in the eastern end of the South China coastal seismic belt and the Qionghai earthquake in the western end of the South China Sea were controlled by the intersection between NW, NE, and NEE faults (Wei *et al*., 2000; Xu *et al*., 2006; Sun *et al*., 2012). The coastal fault zone exhibits similar characteristics to the crustal velocity structure in the eastern and western parts of the Pearl River Estuary. Similarly, the NW-trending faults in the area are intertwined with the coastal fault zone and show the same structural styles as those

* Corresponding author. E-mail: 1424201562@qq.com

from strong earthquake activity areas on both the east and west sides, such as the Chaoshan coastal, Yangjiang, and Leiqiong regions.

A comprehensive and systematic understanding of the geological structure of this area has therefore become important and urgent for scientific assessment of the potential strong earthquake risk. Artificial seismic exploration has been carried out by a number of researchers to assess the two-dimensional crustal structure of the eastern side of the Pearl River Estuary (Yin, 1999; Xia, 2008; Xia *et al*., 2010, 2012; Sun *et al*., 2010; Cao *et al*., 2014). Preliminary geological survey data show different geological and velocity structures on either side of the Pearl River Estuary (Fig.2). Therefore, to strengthen the understanding of the regional structure, a large-scale active source seismic observation experiment was conducted in 2015. The research team was composed of the Seismological Bureau of Guangdong Province, People's Government of Guangdong Province, South China Sea Institute of Oceanology, and China Earthquake Administration Geophysical Exploration Center for the Pearl River Mouth and Offshore. In this paper, we investigate the crustal structure and tectonic implications revealed by deep seismic sounding profiles of the Beijing-Gaoming-Jinwan section in the Pearl River Delta.

2 The Regional Deep Seismic and Tectonic Background

On the large-scale, the Pearl River Estuary area is located in the middle of the South China coastal seismic belt and in a central position on the northern margin of the South China Sea. The eastern side of the area is the fast convergence zone between the NW Philippine Sea Plate and Eurasian Plate (Yu *et al*., 1999). The western side is a shear zone (Simens *et al*., 2007), caused by lateral stress along the Red River fault zone, which was influenced by the collision between the South China Block and Indian-Eurasian Plate (Zhou, 2001). The northern margin of the southern South China Sea, along the coastal fault zone, occurs as a dextrally twist as it accommodates the horizontal stress between the two sides (Sun *et al*., 2012). The coastal fault zone is a deep fault in the northern margin of the South China Sea (Liu *et al*., 1981, Fig.1), although there are many different views on its structural properties (Li *et al*., 1992; Zeng, 1992; Yao, 1994; Wu, 1998; Xu *et al*., 2006). It has been concluded that the fault zone is the boundary between the normal continental crust in South China and the thinning continental margin of the northern margin of the South China Sea (Qiu *et al*.,

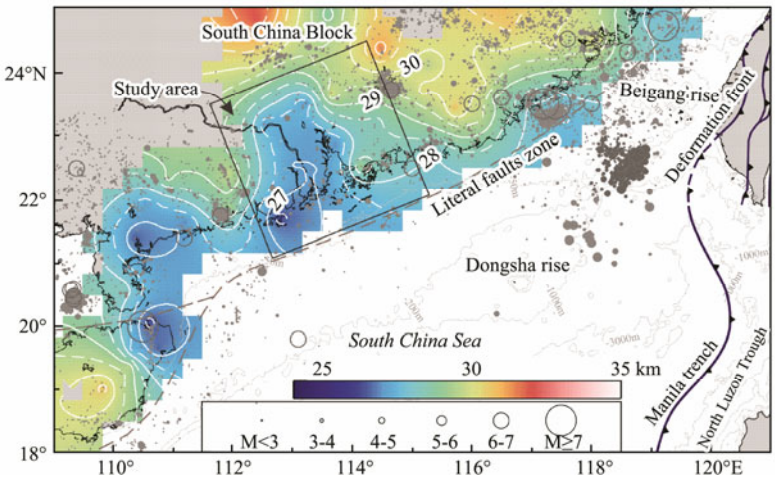

Fig.1 Geographic location and tectonic setting of the study area (Moho depth is based on Huang *et al*., 2014).

2003; Zhao *et al*., 2004) and that it controls the distribution of earthquakes above magnitude 6.0 in the seismic belt of the southern China coast (Xu *et al*., 2006; Sun *et al*., 2012).

On a smaller scale, the Pearl River Delta belongs to a tectonic rift basin in the middle of the southeastern coastal area of the South China Block. The rift basin was developed in a Cretaceous fault block and experienced neotectonic movement. About 40000 years ago, in the Quaternary, the block evolved large-scale polygonal ruptures with multiple fault zones, as shown today (Wei *et al*., 2002). There are many faults located in the basin and at its edge (Wei *et al*., 1992; Liu, 1981, 1985, 1994; Ren *et al*., 2016). These include: the NE-oriented Wuchuan-Sihui, Xinfeng-Conghua-Guangzhou, Kaiping-Enping, and Wuhua-Shenzhen faults; the NW-oriented Xijiang, Baini-Shawan, and Shiziyang faults; and the near EW-oriented coastal zone, Wuguishan, and Guangzhou-Sanshui faults, (Fig.2). These faults cut each other, show multi-stage activity, and control the development of basins in the Pearl River Delta.

In recent years, a series of artificial seismic soundings have been conducted in the Pearl River Estuary area. In 1999, an artificial seismic sounding exploration experiment was conducted from Lianxian to Huidong port (Yin *et al*., 1999). In 2004, two seismic profiles were acquired in the sea offshore Hong Kong (Zhao *et al*., 2004; Xia *et al*., 2008, 2012). In 2010, a seismic survey was carried out in the transition area between the South China and northeastern South China Seas in the Pearl River Estuary (Sun

et al., 2010; Cao *et al*., 2014). Overall, little artificial seismological exploration work has been carried out in the Pearl River Delta region, which has restricted further understanding of the deep tectonic environment in this area.

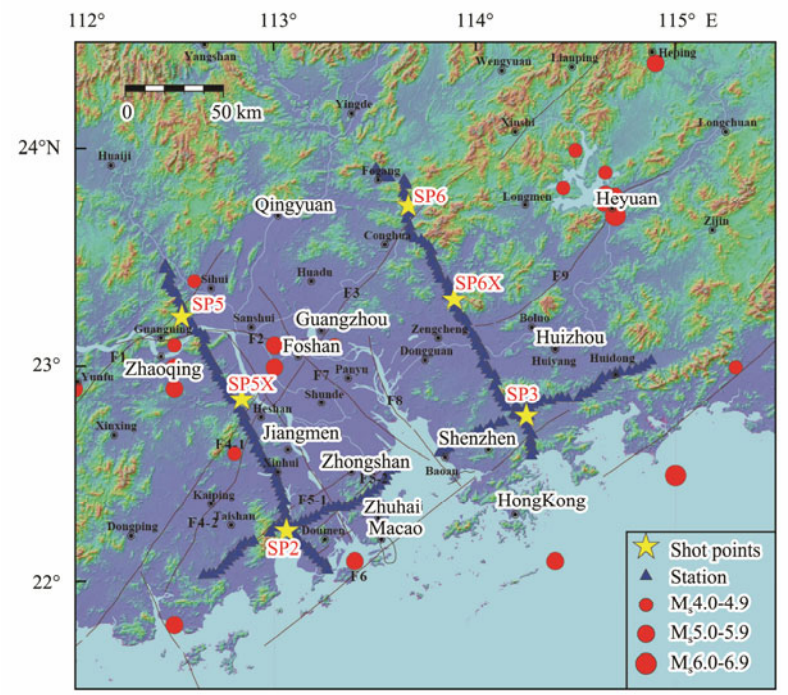

Fig.2 Main faults and historical earthquakes in the Pearl River Delta. F1, Wuchuan-Sihui fault; F2, Guangzhou-Sanshui fault; F3, Xinfeng-Conghua-Guangzhou Fault; F4-1, West branch of Kaiping-Enping fault; F4-2, East branch of Kaiping-Enping fault; F5-1, Wuguishan North foot fault; F5-2, Wuguishan South foot fault; F6, Lianhuashan fault; F7, Baini-Shawan fault; F8, Shiziyang fault; F9, Heyuan fault.

3 Field Work and Data Collection

In 2015, we set up three wide-angle reflection and refraction lines in the Pearl River Estuary, two along a NNW direction (lines L1 and L2, Fig.2) and one along a NEE direction (line L3, Fig.2). The data used in this paper is taken from line L1. The original design of the line was to cut the major NE and NEE faults, including the Kaiping-Enping fault and the Wuchuan-Sihui and Wuguishan fault zones. The acquired seismic data was used to investigate the deep extension in the crustal section of these faults. The northwestern end of line L1 was located at 23°28′22.10′′N and 112°27′20.4′′E, and the southeastern end at 22°3′29.93′′N and 113°15′56.17′′E. According to the original design of the observation system, the coordinates of the model starting-point were 24°1′29.37′′N and 112°3′22.23′′E (Fig.2).

The observation stations on line L1 were located at a spacing of 2.0–2.5 km. A total of 80 three-component digital seismometers were deployed over a total length of about 178 km. Due to the large population and amount of human activity in the Pearl River Delta, the background noise is relatively strong. To reduce the impact of background noise, the stations were deployed as far as possible from local factories, residential areas, and other noise sources. We also built a firm base for the stations to enhance the signal-to-noise ratio. We selected the excitation time of the artificial shot source in a quiet time window from 2:00 to 2:30 am. We conducted three land shots, SP5, SP5X, and SP2 from NNW to SSE (Fig.2) along line L1, using 1.0–2.5 tons TNT as the explosive sources (Table 1).

Table 1 Source parameters of the land shot-points

No.	TNT (kg)	Shot time (2015, Beijing)	Depth of well (m)	Elevation (m)	Longitude	Latitude
SP5	2496	02:00′14.668′′ June 12	30	51	112°32′11.66′′E	23°13′51.19′′N
SP5X	1008	02:10′13.645′′ June 19	71.5	67	112°50′09.83′′E	22°50′59.12′′N
SP2	1992	02:20′16.063′′ June 12	70.5	10	113°03′23.56′′E	22°14′29.10′′N

4 Data Processing and Seismic Phase Characteristics

The seismic data from shots SP5, SP5X, and SP2 were processed and studied, and are presented with a reduction velocity of 6.0 km s^{-1} (Fig.3). The frequency band 2–9 Hz was selected for filtering to improve the seismic signal-to-noise ratio (Fig.3). We identified five sets of seismic phases: Pg, P1, P2, PmP, and Pn (Fig.3). Pg is the refraction wave (first arrival) from the base of the upper crust. Because of the generally shallow burial depth of the base, we clearly detected the reliable first arrival as far as 5 km from the shot-point. We also strengthened the selection

and processing of the receiver station sites, and the shot time window was chosen at the moment of weakest background noise, therefore, the Pg waves can be tracked up to about 140 km from the shot-point. The minimum and maximum reduction times of the Pg waves in the excitation recording section were about 0.2 and 0.8 seconds, respectively. P1 and P2 are the reflected/refracted wave group in the crust, and it can be seen in Fig.3 that these follow the base refraction wave Pg. We identified the reflected wave group P1 and P2, where the P1 wave tracking distance is generally 35–120 km, and the characteristics of the P2 phase are similar to those of phase P1. This occurred from about 40 up to 140 km in shots SP5, SP5X, and SP2.

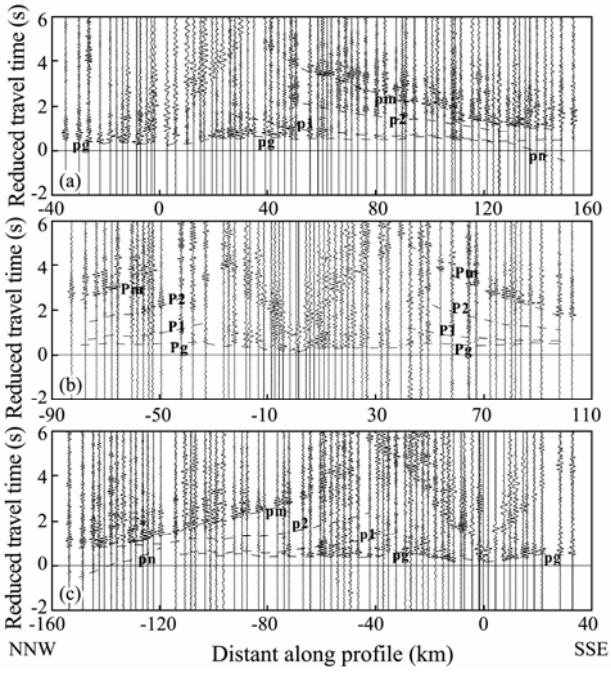

Fig.3 Examples of trace-normalized vertical-component seismic record sections for shots (a) SP5, (b) SP5X, and (c) SP2. A band-pass filter (2–9 Hz) has been applied. Pm and Pn, reflected and refracted waves from the Moho; Pg, waves refracted from the basement; P1 and P2, waves refracted/reflected in crustal interfaces. Reduction velocity is 6.0 km s^{-1}.

PmP is the reflection phase from the Moho interface. This wave group has strong amplitude, which can be tracked continuously, particularly at about 60 km from the shot-point. Pn is the first seismic phase refracted from the top of the upper mantle or Moho interface. Its observation was limited by the length of line L1, and it is only visible at the southeastern end of the SP5 and northwestern end of the SP2 shot records. At offsets greater than 120 km, it can be continuously compared and identified as the first wave.

In summary, the phases Pg, PmP, and Pn in the seismic profile of line L1 can be tracked continuously in this study area, and these phase identifications are clear and reliable. Phases P1 and P2 in the middle layer of the crust are distinct, in both continuity and amplitude, along the record section.

5 Crustal Velocity Structure Model on the Western Side of the Pearl River Estuary

The interpretation of the deep-seismic wide-angle reflection/refraction data is based on the analysis of the seismic phases, and is divided into one-dimensional and two-dimensional cases (Yilmaz, 1994). The conventional one-dimensional interpretation method uses the 'T^2-X^2 method', the 'PLUCH inversion method' (Micheal and Hirn, 1980), and other relevant calculation methods to obtain the average velocity, average depth, and single point reflection of deep layers in the crust. A two-dimensional crustal structure model was established based on the obtained one-dimensional crustal model; using these results and relevant parameters, an initial two-dimensional crust-mantle model was established. Then, ray-tracing and the theoretical seismogram method proposed by Cerveny *et al.* (1984) were used to identify and compare actual observation data from the shot. The reflection and refraction phases were forward-fitted to construct a two-dimensional crustal structure model along the profile, and non-homogeneous medium dynamic ray-tracing, travel-time fitting, and theoretical seismogram calculations were performed. At the same time, after repeated adjustment of the model and processing calculations, the amplitude of the wave group and the characteristics of the measured data achieved the best fit. Through analysis and modeling of the seismic phases detected from the three land shots (Figs.4, 5 and 6), we created the two-dimensional velocity structure and interface morphology of the crust and mantle, and here we give an explanation of fault occurrence in combination with geological structure data (Fig.7).

According to the general understanding of the crustal structure and seismic phase identification from line L1, the crust on the western side of the Pearl River Estuary is divided into upper, middle, and lower. The layer above the C1 (Fig.7) interface, determined by reflective wave group P1, is the upper crust; the layer between the C2 and C1 interfaces, determined by the P2 wave group, is the middle crust; and the bottom layer between C2 and the Moho interface is the lower crust.

5.1 Upper Crust Structure

This upper crust refers to the crustal tectonic layer from the surface to the C1 interface, which was determined by the basement refraction wave Pg and the reflection layer wave P1. Therefore, the upper crust can be subdivided into two sublayer structures.

The first sublayer is the layer between the surface and the interface reflected by refraction wave Pg. The depth and velocity of the interface shows the characteristics of land crystalline basement in the western side of the Pearl River Estuary. Along line L1, the surface depth undulation is slight with most elevations at 0–50 m, and even at an altitude of 85 km is only about 400 m. The depth of the

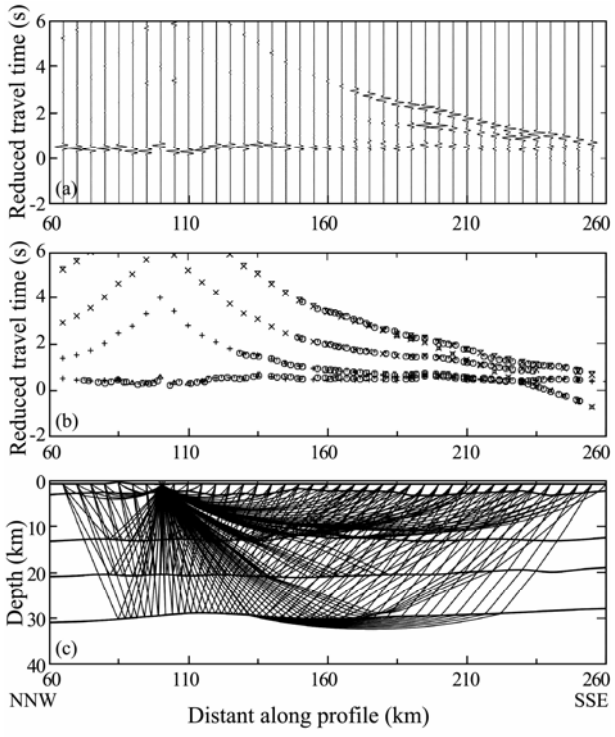

Fig.4 Simulation results of the two-dimensional velocity structure of the crust from SP5. (a) Synthetic section; (b) Time Travel Simulation (○ indicates observation travel time, × indicates synthetic travel time); (c) Model and synthetic ray paths.

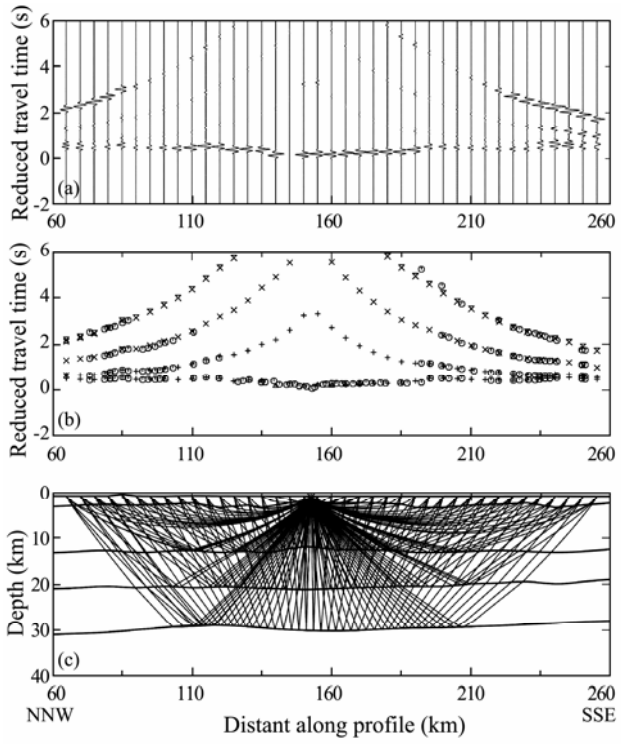

Fig.5 Simulation results of the two-dimensional velocity structure of the crust by SP5X. (a) Synthetic section; (b) Time Travel Simulation (○ indicates observation travel time, × indicates synthetic travel time); (c) Model and synthetic ray paths.

top surface of the crystalline basement varies from 1.5 to 2.5 km, and its fractured top is clearly raised or recessed. The velocity above the top of the crystalline basement has a strong gradient in both the horizontal and vertical directions. Because of the thin Quaternary sedimentary layer on the west side of the Pearl River Estuary, secondary wave development is not obvious.

The second sublayer is the layer between the crystalline basement and the C1 interface, determined by phase P1. The P1 phase is the first group of clear phases after phase Pg, and can be identified via continuous tracking. C1 can be considered as the reflection interface at the bottom of the upper crust. The single point reflection depth, which can reflect the basic form and depth range of the C1 interface, was obtained by modeling phase P1 as recorded by shots SP5, SP5X, and SP2. The pattern of the depth change in the C1 interface and crystalline basement is consistent. The depth of the C1 interface changes from 10.0 to 11.5 km, and the velocity jumps from 6.06–6.12 to 6.18–6.24 km s^{-1}, with a difference of 0.12 km s^{-1} or so. There are more obvious velocity changes in the horizontal direction of the two sublayers, suggesting the distribution of faults in the upper crust on the western side of the Pearl River Estuary.

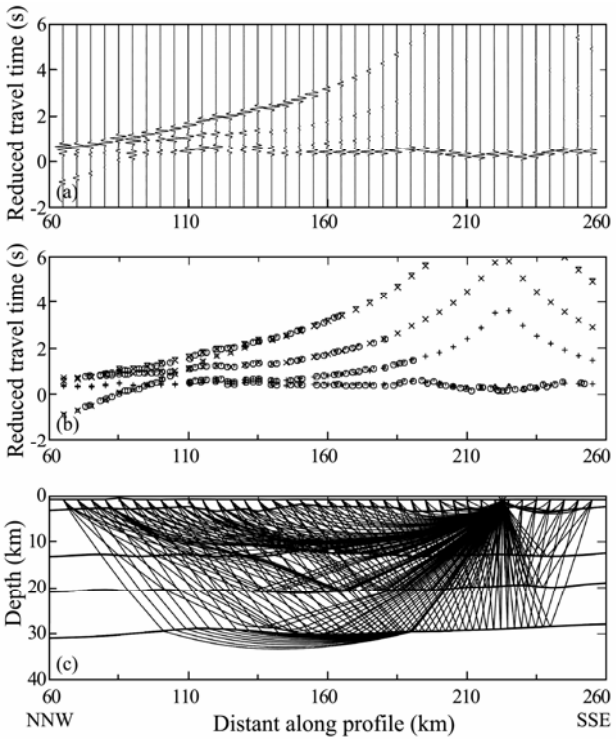

Fig.6 Simulation results of the two-dimensional velocity structure of the crust by SP2. (a) Synthetic section; (b) Time Travel Simulation (○ indicates observation travel time; × indicates synthetic travel time); (c) Model and synthetic ray paths.

5.2 Middle Crust Structure

This layer is defined as the crustal section between the C1 and C2 interfaces, which was determined by the reflected waves P1 and P2 in the crust. The fluctuations in the C2 interface are smaller than in interface C1, reflecting the smaller number of faults that cut into it. The hori-

zontal gradient in the middle crust is not as obvious as in the upper crust, but there are three more obvious low-velocity layers. There is a special low-velocity layer between the Wuchuan-Sihui and Kaiping-Enping faults. The velocity is reversed at a depth of 15.0 km, with a lowest velocity of about 6.05 km s^{-1}. A similar velocity reversal phenomenon occurred on the southern side of the Wuguishan North foot fault, where the velocity of the low-velocity layer was 6.20 km s^{-1}.

The depth of interface C2 changes from 18.0 to 20.0 km, and the velocity jumps from 6.15–6.28 km s^{-1} to 6.55–6.62 km s^{-1}, a difference of 0.32–0.40 km s^{-1}. Interface C2 gradually raises upward from the NNW to the SSE and the coastline, resulting in the middle crust gradually thinning; the thickness gradually reducing from about 9 to about 7 km.

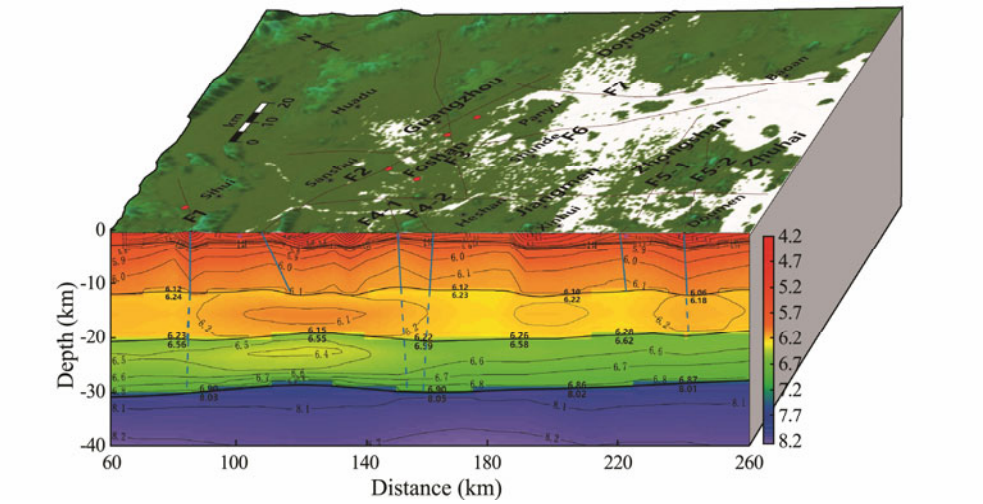

Fig.7 Two-dimensional velocity structure profile of line L1 on the western side of the Pearl River Estuary. The solid blue lines represent the determined faults, and the dashed blue lines indicate the proposed potential fault extensions. The faults, from NNW to SSE, are: F1, Wuchuan-Sihui; F2, Guangzhou-Sanshui; F3, Xinfeng-Conghua-Guangzhou; F4-1, West branch of Kaiping-Enping; F4-2, East branch of Kaiping-Enping; F5-1, Wuguishan North foot; F5-2, Wuguishan South foot; F6, Baini-Shawan; and F7, Shiziyang faults.

5.3 Lower Crust Structure

The lower crust is the crustal layer from interface C2, determined by the reflection wave group P2, to the Moho interface, determined by the reflection wave group Pm. The lower crust has a low-velocity area located under that of the middle crust. This exhibits a minimum velocity of 6.37 km s^{-1} at a distance of 120–130 km and depth of about 21.5 km along line L1.

The Kaiping-Enping fault clearly limits the southern boundary of the low-velocity area in the lower crust, but its northern boundary is less constrained because fewer seismic ray paths coverage. The lower crust velocity structure shows that the northern section structure is relatively complex: the upper and lower velocity contours are characterized by high and low velocities, the overall average velocity is low, and the southern section shows a lower velocity gradient layer.

5.4 Upper Mantle

Phase PmP exhibits strong energy, indicating that the mantle boundary along the profile is a velocity discontinuity (Fig.3). The fluctuations in the Moho are basically the same as those in interface C2, and the Moho interface gradually lifts from the northwest to the southeast. The depth of the Moho is between 27.0 and 30.0 km. The velocity above the Moho interface is about 6.86–6.98 km s^{-1} and below is about 7.98–8.05 km s^{-1}, with a velocity jump up of up to 1.13–1.16 km s^{-1}. This velocity jump is much larger than that between interfaces C1 and C2, which is consistent with Pm and Pn wave groups being dominant in the study area. From the characteristics of the Pn wave, the top of the mantle along the profile is a weaker velocity gradient layer. Along the profile, the Moho interface uplifts between Dinghu and Gaoming, and the area locates almost in the same low-velocity position as the middle and lower crust.

6 Discussion and Conclusions

6.1 Velocity Structural Characteristics Along Profile L1

There are two discontinuity interfaces, C1 and C2, in the crust, two sublayers in the upper crust, and multiple low-velocity anomalies in the two-dimensional velocity profile along line L1. The depth of interface C1 is about 10.0 to 11.5 km. There is a sub-interface, defined as the crystalline basement, located at a depth of about 1.5 to 2.5 km in the upper crust. The depth of interface C2 is about 18.0 to 20.0 km, and the interface moves gradually upward from its NNW end east to the SSE coastline. The thickness of the middle crust gradually reduces from about 8.7 to about 7.5 km. The depth of Moho interface is between 27.0 and 30.0 km, and the crustal thickness gradually decreases from land to coast. It is 30.0 km deep at the NNW end of the section and 27.0 km deep at the SSE end.

Using seismic sounding and gravity data zoning, Hu *et al*. (2014) determined that the Moho depth in South China and the coastal area is from 25 to 38 km. Xia *et al*. (2010) used onshore-offshore seismic soundings to acquire the depth of the Moho interface, about 26–35 km, in the transitional zone between the South China and northern South China Seas. There is a clear trend of shallowing from the NW land side to the coastline, indicating a typical thinning crustal structure. The results obtained in this paper are in good agreement with the above research.

At 120–130 km along line L1, a low-velocity area, lowest velocity 6.05 km s^{-1}, is located at a depth of 15.0 km between interfaces C1 and C2, and another low-velocity area, lowest velocity 6.37 km s^{-1}, is located at a depth of about 21.5 km between C2 and the Moho interface. These low velocities may indicate that the area is composed partly of molten material. Where fractures are located the interface is obviously uplifted or concave, and is consistent with the boundary of the low-velocity anomalies. The low-velocity areas in the middle and lower crust are consistent with the uplifted positions on the Moho interface. The upper mantle and crust may exchange energy and material, resulting in low-velocity anomalies.

6.2 Fault Depth

In the middle crust, the Wuchuan-Sihui, Kaiping-Enping, and Wuguishan Northern faults are limited by the low-velocity area boundary between the C1 and C2 interfaces, indicating that these three faults cut down to at least the C2 interface. In the lower crust, the Kaiping-Enping fault is clearly limited by the southern boundary of the low-velocity area between interface C2 and the Moho. Therefore, the eastern and western branches of the Kaiping-Enping fault are inferred to be within a depth of 30 km, which is consist with the interpretation of gravity and magnetic data by (Ren *et al*., 2016). The Kaiping-Enping fault may be one channel for deep material upwelling, and relates to the tectonic moment of Pearl River Delta rift basin since the Cretaceous.

Interpretation of the Wuguishan Northern foot fault from gravity and magnetic data reveals that the fault depth is 30 km, which is consistent with the southern boundary of the high gravity anomaly area in the Pearl River Delta (Ren *et al*., 2016). The velocity profile shows that along this fault, velocity contour lines show significantly horizontal step in the upper crust, the fault is consistent with the northern boundary of the low-velocity area in the middle crust, and the contour lines are stable in the lower crust. We can only determine that the fault cuts into interface C2 at a depth of at least 20 km.

Revealed at large scale on the ground, the northeast striking Wuchuan-Sihui fault extends to a depth of 30 km, as determined from gravity and magnetic data by (Ren *et al*., 2016). The velocity profile shows contour lines along the fault in the upper crust and other concave velocity lines from the surface to interface C1. The northern boundary of the low-velocity body is in the middle crust.

The lower crust low-velocity body of 6.5 km s^{-1} is as obvious on the north side of the border is it on the south. There is gradually increasing trend, therefore, the Wuchuan-Sihui fault should cut at a shallower depth than the Kaiping-Enping fault.

6.3 Velocity Structure and Earthquake Distribution Characteristics

Earthquake source depth in the Pearl River Delta is mainly concentrated at 5–20 km with the deepest one at about 28 km (Ren *et al*., 2016). From the two-dimensional P-wave velocity structure, the source depth is mainly located in the upper and middle crust above interface C2. Five earthquakes with magnitudes > 5.0 were located within 30 km depth on both sides of line L1, and four of these occurred in the northern area of Gaoming. This is consistent with the low-velocity anomaly areas between interfaces C1, C2, and the Moho. The presence of low-velocity anomalies beneath focal points may contribute to seismic nucleation (Huang, 2001; Huang *et al*., 2004). The middle crust between interfaces C1 and C2 is a transition zone between brittle upper crust and ductile lower crust, and the low-velocity bodies between interfaces C1 and C2, and C2 and the Moho are favorable for stress concentration in the brittle crust above; thus, earthquakes are more likely to occur in the transition zone between the high- and low-velocity layers. Therefore, the north of Gaoming may have moderate potential for strong earthquakes.

In this study, the velocity structures and deep tectonic characteristics of the fault zones provide a new geophysical basis for in-depth understanding of the shallow tectonic relationships and dynamic environment of the western Pearl River Delta.

Acknowledgements

The authors thank Professor Min Xu from South China Sea Institute of Oceanology for improving the quality of the manuscript. Funding for the fieldwork has primarily come from China Earthquake Administration and the People's Government of Guangdong Province. Teams from the Guangdong Earthquake Administration, CEA, South China Sea Institute of Oceanology, CAS, and Geophysical Exploration Center, CEA participated the field work. In addition, the China Seismic Array provided over 60 instruments for observation, and the Geophysical Exploration Center, CEA, provided over 300 instruments for observation. Support for fieldwork was also provided by the People's Government of Guangzhou, the People's Government of Shenzhen, the People's Government of Dongguan, the People's Government of Jiangmen, the People's Government of Foshan, the People's Government of Zhaoqing, the People's Government of Huizhou. The data processing and interpretation is support by the National Natural Science Foundation of China (No. 41676057. The public domain GMT package (Wessel and Smith, 1995) was used to produce some of the figures.

References

Cao, J. H., Sun, J. L., Xu, H. L., and Xia, S. H., 2014. seismological features of the littoral fault zone in the Pear River Estuary. *Chinese Journal of Geophysics*, **57** (2): 498-508 (in Chinese with English abstract).

Cerveny, V., and Psencik, I., 1984. Seis 83-numercal modeling of seismic wavefield in 2-D laterally varying layered structures by the ray method. *Documentation of Earthquake Algorithm. Boulder Colo Report: World Data Center for Solid Earth Geophysical*, **SE-35**: 36-40.

Chen, E. M., and Huang, Y. Y., 1979. Preliminary Study on Qiongzhou earthquake and its seismogenic structure in Hainan Island in 1605. *Seismology and Geology*, **1** (4): 37-44.

China Zoning Map of the Ground Motion Parameters, 2015, GB18306-2015.

Hilde, T. W. C., Uyeda, S., and Kroenke, L., 1977. Evolution of the western Pacific and its margin. *Tectonophysics*, **38** (s1-2): 145-152.

Hu, W. J., Hao, T. Y., Qin, J. X., Li, Z. W., Jiang, W. W., Jiang, D. D., Xing, J., Hu, L. T., Xu, Y., and Lei, S. M., 2014. Moho depth and deep crustal structure in the land and seas of China and adjacent areas: An example of the Altay-Bash Channel profile. *Chinese Journal of Geophysics*, **57** (12): 3932-3943 (in Chinese with English abstract).

Huang, H. B., Guo, X. W., Xia, S. H., and Qiu, X. L., 2014. Crustal thickness and Poisson's ratio in the coastal of South China. *Chinese Journal of Geophysics*, **57** (12): 3896-3906 (in Chinese with English abstract).

Huang, J. L., Zhao, D. P., and Zheng, S. H., 2001. Seismic Tomography of the Sichuan-Yunnan active tectonic region. *Chinese Journal of Geophysics*, **44** (S1): 127-136 (in Chinese with English abstract).

Huang, J. L., and Zhao, D. P., 2004. Crustal heterogeneity and seism tectonics of the region around Beijing, China. *Tectonophysics*, **385** (1-4): 159-180 (in Chinese with English abstract).

Kenner, S. J., and Segall, P., 2000. A mechanical model for intraplate earthquakes: Application to the New Madrid seismic zone. *Science*, **289** (5488): 2329-2332.

Li, T. G., Qiu, Y., and Yao, Y. J., 1992. Geomorphic features. In: *Geophysical Characteristics of Chinese Waters and Neighborhoods*. Liu, G. D., ed., Science Press, Beijing, 248-271 (in Chinese).

Liu, Y. X., 1985. Activity faults in the South China Sea coastal. *Marine Geology and Quaternary Geology*, **5** (3): 11-21 (in Chinese with English abstract).

Liu, Y. X., 1994. *Neotectonics and Crustal Stability of South China Sea*. Science Press, Beijing, 85-107 (in Chinese).

Liu, Y. X., 1981. *Fault Tectonic Analysis of Coastal Areas in South China*. Earthquake Press, Beijing, 19-49 (in Chinese).

Micheal, B., and Hirn, A., 1980. Velocity-depth estimation from wide angle seismic reflection arrivals. *Annuals de Geophysique*, **36** (1): 107-118.

Qiu, X. L., Zhao, M. H., Ye, C. M., Wang, T. K., Wang, P., Zhang, Y. X., Xia, K. Y., and Lee, C. S., 2003. Ocean bottom seismometer and onshore-offshore seismic experiment in northeastern South China Sea. *Geotectonica et Metallogenia*, **24** (4): 295-302.

Ren, Z. H., Luo, Z. N., and Hua, W., 2002. Structural characteristics of seismicity and its great earthquake situation at the junction of Guangdong, Fujian and Jiangxi provinces. *South China Earthquake*, **22** (3): 28-38.

Ren, Z. H., Ye, X. W., Huang, J. T., Qiao, J. H., Li, Y. G., Wei, M. C., Liao, G. J., Bi, L. S., and Hua, W., 2016. *Deep Fault System and Strong Earthquake Structure in Coastal Areas of South China*. Guangdong Science and Technology Press, Guangzhou, 1-22 (in Chinese).

Simons, W. J. F., Socquet, A., Vigny, C., Ambrosius, B. A. C., Abu, S. H., Promthong, C., Subarya, C., Sarsito, D. A., Matheussen, S., Morgan, P., and Spakman, W., 2007. A decade of GPS in southeast Asia: Resolving Sunda land motion and boundaries. *Journal of Geophysical Research Solid Earth*, **112** (B6): 623-626.

Sun, J. L., Xia, S. H., Xu, H. L., Qiu, X. L., and Zhu, J. J., 2010. Introduction of the onshore-offshore joint deep seismic prospecting in the northern South China Sea. *South China Journal of Seismology*, **30** (s1): 45-52 (in Chinese with English abstract).

Sun, J. L., Xu, H. L., and Zhan, W. H., 2012. Activity and triggering mechanism of seismic belt along the northern South China Sea continental margin. *Journal of Tropical Oceanography*, **31** (3): 40-47 (in Chinese with English abstract).

Talwani, P. A., 2014. Unified model for intraplate earthquakes. In: *Intraplate Earthquakes*. Talwani, P., ed., Cambridge University Press, Cambridge, 275-302.

Talwani, P., 2016. On the nature of intraplate earthquakes. *Journal of Seismology*, **21** (1): 47-68.

Wei, B. L., Chen, R. F., and Huang, R. H., 2000. *An Introduction to Seismological Structure in Guangdong Province*. Earthquake Press, Beijing, 226pp (in Chinese).

Wei, B. L., Feng, X. M., Chen, D. G., Huang, R. H., Wu, S. P., Ding, X. R., and Hu, J. C., 2001. *Characteristics of Seismic Activity in the Southeast Coast*. Earthquake Press, Beijing, 398-437 (in Chinese).

Wei, B. L., Sun, C. C., Qin, N. G., Wen, Z. G., Liu, T. P., Chen, W. G., and Wei, H. Y., 2002. *Study on Seismic Activity and Prediction in the Pearl River Delta*. Earthquake Press, Beijing, 1-11 (in Chinese).

Wu, J. M., 1998. A number of issues on the South China Sea geological structure. In: *Inch Dan Set (to Celebrate the 50th Anniversary of Academic Work for Liu Guangding Academician Papers*). Chen, R., ed., Science Press, Beijing, 61-73 (in Chinese).

Xia, S. H., Qiu. X, L, Zhao, M. H., Xu, H. L., Ye, C. M., and Chan, Y. W., 2008. Investigation on deep structure along the onshore-offshore seismic profile near Hong Kong. *Progress in Geophysics*, **23** (5): 1389-1397 (in Chinese with English abstract).

Xia, S. H., Qiu, X. L., Zhao, M. H., Xu, H. L., and Shi, X. B., 2010. Analysis of crustal average velocity and moth depth beneath the onshore-offshore transitional zone in the northern South China Sea. *Journal of Tropical Oceanography*, **29** (4): 63-70 (in Chinese with English abstract).

Xia, S. H., Qiu, X. L., Tong, C. H., Xu, H. L., and Zhao, M. H., 2012. Three-dimensional tomographic model of the crust beneath the Hong Kong region. *Geology*, **40** (1): 59-62.

Xu, H. L., Qiu, X. L., and Zhao, M. H., 2006. Crustal structure and source structure of epicentral area in the South China Sea earthquake (M = 7.5) in the northeastern South China Sea. *Chinese Science Bulletin*, **51** (B11): 83-91 (in Chinese with English abstract).

Xu, J., Zhang, J., Zhou, B. G., and Chen, G. G., 2006. Study on the coastal fault zone in the northern South China Sea. *South China Earthquake*, **26** (4): 8-13 (in Chinese with English abstract).

Yao, B. C., Zeng, W. J., and Chen, Y. Z., 1994. The crustal struc-

ture in the eastern part of the northern margin of the South China Sea. *Chinese Journal of Geophysics*, **37** (1): 27-35 (in Chinese with English abstract).

Yilmaz, O., 1994. *Seismic Data Processing*. Translated by Huang, X. D., Yuan, M. D., Petroleum Industry Press, Beijing, 1-22.

Yin, Z. X., Lai, M. H., Xiong, S. B., Liu, H. B., Teng, J. W., and Kong, X. R., 1999. Crustal structure and velocity distribution based on deep seismic sounding along the Lianxian-Boluo-Gangkou profile in southern China. *Chinese Journal of Geophysics*, **42** (3): 383-392 (in Chinese with English abstract).

Yu, S. B., Kuo, L. C., Punongbayan, R. S., and Ramos, E. G., 1999. GPS observation of crustal deformation in the Taiwan-luzon region. *Geophysical Research Letters*, **26** (7): 923-926.

Zeng, W. J., 1992, Guangzhou-Palawan geonomy fracture. In: *Geophysical Characteristics of Chinese Waters and Neighborhoods*. Liu, G. D., ed., Science Press, Beijing, 272-288 (in Chinese).

Zhao, M. H., Qiu, X. L., Ye, C. M., Xia, J. Y., Huang, C. L., Xie, J. B., and Wang, P., 2004. Analysis on deep crustal structure along the onshore to offshore seismic profile across the Binhai (Littoral) fault zone in northeastern South China Sea. *Chinese Journal of Geophysics*, **47** (5): 845-852 (in Chinese with English abstract).

Zhong, Y. J., and Ren, Z. H., 2003. Study on seismogenic tectonic of Yangjiang M6.4 earthquake. *Journal of Geodesy and Geodynamics*, **23** (4): 92-98.

Zhou, S. Y., Wu, Y., Shi, S. Y., and Yang, F. P., 2001. Integrated research on current crustal movement and earthquake dynamics in marginal sea, southeast of China continent. *Measurement and Geodynamics*, **21** (1): 1-14.

(Edited by Chen Wenwen)